Journal of Asian Earth Sciences xxx (2008) xxx–xxx

Contents lists available at ScienceDirect

Journal of Asian Earth Sciences

journal homepage: www.elsevier.com/locate/jaes

Syn-kinematic emplacement of the Pangong metamorphic and magmatic complex along the Karakorum Fault (N Ladakh)

Y. Rolland [a,*], G. Mahéo [b], A. Pêcher [c], I.M. Villa [d,e]

[a] Géosciences Azur, CNRS Université de Nice Sophia Antipolis, 28 Av. de Valrose, BP 2135, 06103 Nice Cedex 2, France
[b] Université de Lyon 1, Laboratoire de Sciences de la Terre and ENS Lyon, F-69622 Villeurbanne, France
[c] LGCA-LGIT, UPRES-A5025 CNRS, Université J. Fourier, Maison des Géosciences, BP 53, 38041 Grenoble, France
[d] Institut für Geologie, Baltzerstrasse 3, 3012 BERN, Switzerland
[e] Dipartimento di Scienze Geologiche e Geotecnologie, Università di Milano Bicocca, 20126 Milano, Italy

ARTICLE INFO

Article history:
Received 20 March 2008
Accepted 26 March 2008
Available online xxxx

Keywords:
Karakorum Fault
Granulites
Magmatism
Himalaya

ABSTRACT

This paper investigates the age, *P–T* conditions and kinematics of Karakorum Fault (KF) zone rocks in the NW part of the Himalaya–Karakorum belt. Granulite to greenschist facies assemblages were developed within the KF zone during strike-slip shearing. The granulites were formed at high temperature (800 °C, 5.5 kbar), were subsequently retromorphosed into the amphibolite facies (700–750 °C, 4–5 kbar) and the greenschist facies (350–400 °C, 3–4 kbar). The Tangtse granite emplaced syn-kinematically at the contact between a LT and the HT granulite facies. Intrusion occurred during the juxtaposition of the two units under amphibolite conditions. Microstructures observed within the Tangtse granite exhibit a syn-magmatic dextral S–C fabric. Compiled U–Pb and Ar–Ar data show that in the central KF segment, granulite facies metamorphism occurred at a minimum age of 32 Ma, subsequent amphibolite facies metamorphism at 20–18 Ma. Further shearing under amphibolite facies (650–500 °C) was recorded at 13.6 ± 0.9 Ma, and greenschist-facies mica growth at 11 Ma. These data give further constrains to the age of initiation and depth of the Karakorum Fault. The granulite-facies conditions suggest that the KF, accommodating the lateral extrusion of Tibet, could be at least a crustal or even a Lithosphere-scale shear zone comparable to other peri-Himalayan faults.

1. Introduction

North of the Himalayan belt, in response to the India–Asia collision, the eastward extrusion of the Tibetan bloc is accommodated by major strike-slip faults (Red River Fault, Altyn Tagh Fault, Karakorum Fault (KF); Tapponnier and Molnar, 1977; Tapponnier et al., 1986; Peltzer and Tapponnier, 1988; Armijo et al., 1989). Some of these strike-slip faults have recently been shown to be deeply rooted. Actually, seismic tomography across the Altyn Tagh Fault has evidenced a negative *P*-wave anomaly below the fault down to 140 km depth, interpreted as lithospheric scale shearing (Wittlinger et al., 1998). Along the Red River Fault, syn-shearing formation and exhumation of HT rocks is indicative of at least a crustal-scale structure (Harrison et al., 1992; Lacassin et al., 1997; Leloup et al., 1995). The trans-crustal to trans-lithospheric character of these faults may allow thermal advection by magma guided along the fault ("leaky" transcurrent fault), but shear heating may also be invoked (Leloup et al., 1999). However, the scale of the Karakorum Fault, SE boundary of Tibet, is unknown, and the importance of lateral extrusion of Tibet along this fault is much discussed. The published estimates of right-lateral motion range from 66 to 1000 km (Peltzer and Tapponnier, 1988; Liu et al., 1992; Liu, 1993; Searle, 1996; Searle et al., 1999; Murphy et al., 2000). More recently, several studies focussed on the central part of the KF have proposed right-lateral displacements of 280–300 km based on the offset of suture zones (Rolland and Pêcher, 2001; Lacassin et al. (2004a,b)). These estimates are opposed to smaller estimates of 120 km based on the correlation of the Baltoro Batholith in Karakorum and the Tangtse granite in the Pangong Range (Searle, 1996; Searle et al., 1999; Searle and Phillips, 2004; Phillips et al., 2004). However, some authors consider that the Tangtse granite is not offset by but is rather emplaced within the KF (Lacassin et al., 2004). In this paper, we present additional structural, metamorphic, geochronological and geochemical data on the Tangtse granite as well as on adjacent HT metamorphic rocks within the Pangong Range. The following questions are addressed by this paper: (1) is the Tangtse granite offset by or emplaced within the KF?; (2) What is the significance of the HT metamorphism?

* Corresponding author. Tel.: +33 4 92076586; fax: +33 4 92076816.
E-mail address: yrolland@unice.fr (Y. Rolland).

1367-9120/$ - see front matter © 2008 Elsevier Ltd. All rights reserved.
doi:10.1016/j.jseaes.2008.03.009

2. Analytical methods and procedures

Nine igneous rocks were analysed for major elements (Table 1) using X-Ray fluorescence (XRF) at the University C. Bernard of Lyon. Loss on ignition (LOI) was determined by heating the sample at 1000 °C for 30 min.

Mineral analyses, presented in Table 2, were obtained on a Cameca SX-100 microprobe at the University Blaise Pascal of Clermont–Ferrand. Counting time was 10 s. per element; the accelerating potential was 20 kV for a sample current of 20 nA. Natural silicates were used as standards.

To determine pressure and temperature (*P–T*) conditions, we have used two complementary approaches in addition to analyse equilibrated mineral parageneses. Metapelites can be described in the KFMASH system (Spear, 1993). Metamorphic equilibrium and metamorphic reactions, deduced from textural relationships between the different mineral species, in thin sections, have been first projected on the KFMASH petrogenetic grids defined by Spear and Cheney (1989), completed by Vielzeuf and Holloway (1988) and Le Breton and Thompson (1988). Complementary *P–T* estimates have been obtained using cationic exchanges reactions between garnet and other minerals. Uncertainties for the garnet biotite thermometry correspond to the standard deviation (at the 2σ-level) calculated for each selected calibration on each sample. Uncertainties in pressure, also corresponding to the standard deviation (at the 2σ-level), were calculated for each selected calibration with the previously calculated average temperature interval for the same biotite–garnet pair.

Metabasites have a calc-akaline compositions, ranging from basalts to andesites (see Section 4). They can thus be described in the CaFMASH system. As the grossular content of garnet is very high, pressures calculated using cationic exchange reactions between garnet and other minerals by may be overestimated. We therefore used the Thermocalc software of Powell and Holland (1988) and Holland and Powell (1990) in complement to projections on the CaFMASH grid and cationic exchange reactions for temperature estimates. Uncertainties, drawn as ellipses on the *P–T* diagram, are given at the 2σ-level. These uncertainties are due to (i) the variability of microprobe data, and (ii), the confidence interval of thermodynamic data variability for a given chemical composition.

Two samples were selected for amphibole Ar–Ar dating. They were irradiated at the TRIGA reactor in Pavia, and analysed at the isotope geology laboratory of Bern University. The sample was heated in a double vacuum resistance furnace. Ar was analysed in a MAP 215-50B rare gas spectrometer. The Ar–Ar results are presented in Table 3, for more details about analytical procedures see (Villa et al., 2000).

3. Geological setting and structural observations

The Pangong Range is a 100 km long–5 to 10 km wide massif located between two branches of the Karakorum fault (Fig. 1). It is constituted by two tectonic units: a central granulite facies core and an amphibolitic cortex (Rolland and Pêcher, 2001; Rolland, 2002). The granulite facies core Pangong Range is mainly comprised by metabasites and limestones, while the amphibolite facies rim is composed of metapelitic schits and gneisses and some metabasic rocks found as decametre to hectometre-scale lenses. The limit between the two zones is a sharp fault probably still active. The Tangtse granite is emplaced as an "injection complex" (Weinberg and Searle, 1998), a complex network of dikes, at the boundary of the two zones. The Pangong Range is located in an area where the Karakorum fault trend shifts from ~155N° in the Nubra area to ~N140° along the Pangong Lake (Fig. 1). In the context of the dextral strike-slip motion of the Karakorum fault the Pangong Range is thus a transpressive zone (Weinberg et al., 2000). However, existence of triangular facets and deformation of glacial valleys are indicative of recent dextral plus normal motion on the eastern boundary of the Pangong range.

Our study focuses on the central portion of the fault (Fig. 1), where the fault fringes the Karakorum terrain to the NW, striking along the Nubra Valley, and reactivates the Shyok Suture to the SW, along the Shyok and Pangong valleys. The structural pattern at a regional scale shows a partitioning between the fault zone and the tectonic blocs on each side. Strike-slip strain is concentrated in a narrow zone (2–10 km), clearly evidenced by dextral S–C bands (e.g., Matte et al., 1996), while outside of this zone, NW–SE oriented structures are compatible with a context of NE–SW shortening (Fig. 2). Along the Nubra valley, the structural pattern (Fig. 2A) is featured by very steep foliation parallel with the KF and plunging 70–80° east. Mineral lineation is plunging preferentially to the SE (mean value, 140°SE25). Fold lineations axes, which are equally parallel to the fault strike, plunge moderately to the NW (mean of 20°). The association of C–S fabrics (Berthé et al., 1979), parallel to the fault, with a SE dipping lineation show that the last deformational event corresponds to a strong strike-slip component, and a slight uplift of the western side of the fault.

In the granulite and amphibolite facies units of the Pangong Range, the foliation planes are subvertical and also parallel with the local trend of the Karakorum fault, i.e., N140° (Fig. 2B), but the mineral lineation is rather plunging NW of about 20°. Associ-

Table 1
XRF geochemical data of Pangong Range metamorphic rocks, locations shown on Fig. 1

No. Sample (in wt%)	LK96/1C	LK96/6A	LK96/6B	LK96/6C	LK96/6D (duplicate)	LK96/6D	LK96/7A	LK96/8A	LK96/8B	LK96/8C
SiO_2	70.36	63.21	71.57	64.24	61.66	62.64	55.59	52.26	67.91	48.29
TiO_2	0.57	0.43	0.60	0.67	0.69	0.70	0.86	1.07	0.53	1.27
Al_2O_3	11.94	14.04	12.15	15.48	14.94	14.56	16.08	13.53	16.48	14.94
Fe_2O_3t	4.69	4.95	3.96	5.85	6.96	6.68	10.06	8.66	2.26	9.78
MnO	0.11	0.16	0.07	0.08	0.11	0.11	0.20	0.15	0.03	0.21
MgO	1.82	2.10	1.73	2.58	2.86	3.05	5.17	9.24	0.55	7.58
CaO	6.57	10.38	4.85	5.84	8.41	8.47	8.45	9.12	2.15	10.60
Na_2O	1.58	1.88	2.90	2.56	1.43	1.30	2.55	2.63	3.51	2.87
K_2O	1.56	0.48	0.73	1.81	1.81	1.86	0.08	1.76	5.31	1.20
P_2O_5	0.13	0.10	0.16	0.15	0.17	0.16	0.09	0.30	0.17	0.28
LOI	0.59	1.47	0.43	0.58	0.85	0.63	0.51	1.21	0.43	0.86
H_2O^-	0.08	0.01	0.04	0.08	0.03	0.14	0.17	0.00	0.03	1.64
Total	100.00	99.21	99.19	99.92	99.92	100.30	99.81	99.93	99.36	99.52

Please cite this article in press as: Rolland, Y. et al., Syn-kinematic emplacement of the Pangong metamorphic and magmatic complex along the Karakorum Fault (N Ladakh) ..., Journal of Asian Earth Sciences (2008), doi:10.1016/j.jseaes.2008.03.009

Table 2
Electron microprobe chemical analyses of principal representative minerals

Minerals:	cpx	Parg.	Ged.	Ant.	Scp.	Biotite		Plagioclase			Rutile spin. Garnet							Cord.	And.		
Assemblage (in wt%)	1	1	2	2	1	1	3	4	1	3	4	2	2	1	2	3	4	5	5	5	5
SiO_2	51.73	41.39	45.55	54.13	45.45	37.01	35.42	35.18	47.30	45.92	56.62	0.01	–	37.69	40.96	37.16	37.36	47.48	46.86	37.25	36.73
Al_2O_3	1.94	14.09	18.32	5.98	27.46	16.10	16.72	19.42	33.16	33.84	28.66	0.04	0.03	21.43	23.11	21.44	21.45	31.42	31.14	62.48	62.58
MgO	12.69	9.57	19.98	23.81	0.05	9.66	10.29	8.66	0.02	0.01	–	–	4.22	2.87	13.38	1.93	3.25	7.17	7.21	0.04	0.05
FeO	6.61	15.21	11.06	11.97	0.11	19.40	19.94	19.23	0.10	0.12	0.087	0.10	38.99	19.00	19.52	20.37	30.88	9.28	9.48	0.32	0.38
Fe_2O_3	2.47	0.36	–	–	–	–	–	–	–	–	–	–	–	2.31	–	2.05	–	–	–	–	–
MnO	0.15	0.11	0.17	0.08	–	0.26	0.34	0.23	0.05	0.02	–	–	0.22	1.31	0.44	5.96	5.16	0.66	0.67	–	0.01
Cr_2O_3	0.02	–	–	–	–	–	–	–	0.03	–	–	–	–	0.11	–	–	–	–	–	–	–
TiO_2	0.11	1.19	0.37	0.16	–	3.73	2.44	2.81	–	–	–	99.92	55.93	0.17	0.02	–	0.06	0.04	0.00	0.03	0.08
CaO	23.68	12.08	0.88	0.63	18.64	0.08	0.03	0.04	16.95	17.04	10.4	0.02	0.05	15.39	3.66	11.38	2.94	0.06	0.12	0.01	0.01
Na_2O	0.47	1.15	1.24	0.28	2.95	0.12	0.14	0.23	1.96	1.95	5.947	–	–	–	0.03	–	–	0.82	0.84	0.07	0.03
K_2O	0.02	2.11	0.01	0.02	0.09	9.57	9.49	9.51	0.10	0.05	0.102	0.02	0.01	0.02	–	–	0.01	–	0.04	0.02	0.02
Total	99.88	97.31	97.58	97.05	94.75	95.94	94.82	95.31	99.66	98.94	101.8	100.1	99.45	100.3	101.1	100.3	101.1	96.91	96.37	100.2	99.88
																		18	18	20	20
Si	1.97	6.26	6.33	7.52	6.71	5.61	5.47	5.36	2.19	2.14	2.51		1.65 Ti	5.94	6.02	5.94	5.94	5.02	4.99	4.02	3.98
Al	0.09	2.51	3.00	0.98	4.78	2.88	3.04	3.49	1.81	1.86	1.49		1.2 Fe	3.98	4.00	4.04	4.02	4.78	4.78	8.74	8.79
Ti		0.13	0.04	0.02		0.43	0.28	0.32					0.15 Mg	0.02			0.01				0.01
Fe^{2+}	0.21	1.92	1.29	1.39	0.01	2.46	2.57	2.45						2.50	2.40	2.72	4.11	1.00	1.03	0.03	0.04
Fe^{3+}	0.07	0.05												0.09	0.08	0.00					
Mg	0.72	2.16	4.14	4.93		2.18	2.37	1.97						0.67	2.93	0.46	0.77	1.38	1.40	0.01	0.01
Ca	0.97	1.96	0.13	0.09	2.95				0.84	0.85	0.49			2.60	0.58	1.95	0.50				
Mn		0.01	0.02	0.01		0.03	0.04	0.03						0.17	0.05	0.81	0.69	0.07	0.07		
Cr																					
Na	0.03	0.34	0.33	0.08	0.85	0.04	0.04	0.07	0.18	0.18	0.51							0.20	0.21	0.02	0.01
K		0.41			0.02	1.85	1.87	1.85	0.01		0.01										
	jd = 5.68$(Na+K)_A$ = 0.7		0.3	0.02		XFe:0.53	0.52	0.55						% Alm = 41.45	40.23	45.84	67.62 XFe:	0.42	0.42	0.75	0.80
	Wo = 47.44 $(Na)_A$ = 0.3		0.3	0.01	XMe = 77.5			% Ab = 0.17	0.17	0.51				% Gro = 43.01	9.67	32.81	8.25				
	En = 35.38 $(Na)_B$ = 0.0		0.04	0.06	Na/K = 0.98			% An = 0.82	0.83	0.49				% Py = 11.14	49.18	7.75	12.69				
	Fs = 11.50 X_{Mg} = 0.52		0.76	0.78	Na/Ca = 0.29			% Or = 0.006		0.006				% Spes = 2.88	0.92	13.59	11.44				

cpx, clinopyroxene; parg, pargasite; ged, gedrite; ant, anthophyllite; scp, scapolite; spin, spinel; jd, jadeite; wo, wollastonite; en, enstatite; me, meionite; ab, albite; an, anorthite; or, orthose; alm, almandine; gro, grossular; py, pyrope; spes, spessartine; Cord, cordierite; And, andalusite.

Table 3
$^{40}Ar/^{39}Ar$ age data for hornblende from samples L450 and L441 (Pangong Range)

Temperature (°C)	^{40}Ar(mol)	Error ^{40}Ar	^{39}Ar (mol)	Error ^{39}Ar	% $^{39}Ar/^{40}Ar$	^{38}Ar (mol)	Error^{38}Ar	Cl	^{37}Ar (mol)	Error ^{37}Ar	^{36}Ar (mol)	Error ^{36}Ar	Ca/K	Error Ca/K	Age (Ma)	Age error
Sample L450																
st1, 713	1.05E−08	9.00E−13	4.63E−11	2.40E−13	5.02E+00	8.85E−12	3.00E−13	2.75E−12	1.37E−10	3.20E−02	2.99E−11	1.50E−13	5.94E+00	5.60E−02	48.60	1.30
st2, 918	3.26E−09	4.00E−13	7.02E−11	2.50E−13	7.62E+00	9.17E−12	1.80E−13	7.03E−12	8.43E−10	8.00E−02	7.88E−12	1.50E−13	2.42E+01	1.20E−01	18.64	0.83
st3, 975	6.13E−09	7.90E−13	2.25E−10	2.70E−13	2.45E+01	2.99E−11	2.60E−13	2.64E−11	3.65E−09	2.80E−01	8.14E−12	1.40E−13	3.27E+01	9.50E−02	23.38	0.22
st4, 1035	2.19E−09	4.60E−13	6.94E−11	2.10E−13	7.53E+00	9.70E−12	2.10E−13	8.39E−12	1.12E−09	1.00E−01	3.76E−12	1.60E−13	3.26E+01	1.40E−01	22.04	0.81
st5, 1086	6.74E−09	1.30E−12	2.58E−10	2.60E−13	2.81E+01	3.39E−11	2.20E−13	2.98E−11	4.27E−09	3.30E−01	1.02E−11	2.00E−13	3.34E+01	9.50E−02	20.66	0.27
st6, 1150	3.03E−09	8.20E−13	9.76E−11	1.40E−13	1.06E+01	1.26E−11	3.20E−13	1.10E−11	1.60E−09	1.30E−01	4.12E−12	1.40E−13	3.31E+01	1.00E−01	26.05	0.49
st7, 1285	2.91E−09	9.60E−13	7.28E−11	2.00E−13	7.91E+00	8.77E−12	3.00E−13	7.31E−12	1.18E−09	9.60E−02	4.41E−12	1.60E−13	3.29E+01	1.30E−01	30.60	0.80
st8, 1388	4.33E−09	1.20E−12	8.10E−11	2.20E−13	8.79E+00	1.06E−11	1.30E−13	8.21E−12	1.33E−09	1.10E−01	8.97E−12	1.40E−13	3.33E+01	1.30E−01	28.91	0.63
Sample L441																
st1, 735	7.54E−09	1.90E−12	8.68E−11	2.00E−13	1.398	1.23E−11	2.70E−13	7.73E−12	1.45E−10	8.68E−13	1.92E−11	1.50E−13	3.35E+00	2.00E−02	50.18	1.20
st2, 935	7.57E−09	4.00E−12	7.45E−10	7.10E−13	12.002	2.65E−10	6.00E−13	2.54E−10	2.93E−09	8.18E−12	1.14E−11	1.50E−13	7.89E+00	2.20E−02	13.91	0.13
st3, 975	1.09E−08	5.50E−13	1.51E−09	1.30E−12	24.280	5.59E−10	1.00E−12	5.41E−10	5.24E−09	1.43E−11	9.66E−12	1.40E−13	6.96E+00	1.90E−02	13.09	0.06
st4, 1004	1.07E−08	1.40E−12	1.66E−09	1.50E−12	26.723	6.16E−10	1.10E−12	5.97E−10	5.23E−09	1.49E−11	5.68E−12	1.10E−13	6.32E+00	1.80E−02	13.25	0.04
st5, 1060	9.08E−09	8.20E−13	1.40E−09	1.30E−12	22.481	4.71E−10	8.60E−13	4.55E−10	4.14E−09	1.18E−11	2.99E−12	8.30E−14	5.94E+00	1.70E−02	14.27	0.03
st6, 1085	2.42E−09	4.50E−13	3.43E−10	3.20E−13	5.518	1.13E−10	2.90E−13	1.09E−10	1.11E−09	3.25E−12	1.15E−12	2.00E−13	6.47E+00	1.90E−02	14.75	0.30
st7, 1110	1.16E−09	9.90E−12	1.24E−10	2.60E−13	1.997	4.10E−11	1.20E−13	3.93E−11	4.97E−10	1.73E−12	1.90E−12	1.20E−13	8.03E+00	2.80E−02	12.10	0.65
st8, 1180	1.22E−09	2.30E−12	1.54E−10	5.50E−13	2.473	5.16E−11	1.80E−13	4.95E−11	1.10E−09	6.04E−12	2.70E−12	1.20E−13	1.44E+01	7.90E−02	7.81	0.51
st9, 1314	8.34E−10	8.30E−13	9.01E−11	1.70E−13	1.451	3.08E−11	2.40E−13	2.97E−11	5.38E−10	1.97E−12	7.10E−13	1.30E−13	1.20E+01	4.40E−02	17.27	0.78
st10, 1410	9.10E−10	5.50E−13	1.04E−10	2.30E−13	1.675	3.59E−11	1.80E−13	3.43E−11	4.84E−10	1.87E−12	2.55E−12	1.20E−13	9.32E+00	3.60E−02	4.39	0.74

ated S–C fabrics are indicative of dextral motion associated with relative exhumation of the eastern side of the fault. The Tangtse granite is a complex network of dikes, intrusive at the contact between the amphibolite and granulite units, and is affected by syn to post-granite crystallisation C–S deformation (Fig. 3). In contrast with the Nubra area, the similarly with the Pangong area, the mineral lineations dip towards the NW (dipping a mean of 30°NW). In this area as in the Pangong Range, relative to the Nubra area, the last deformational event corresponds to a slightly less strong strike-slip component, with an exhumation of the eastern side of the fault.

Within the northern Ladakh terrain margin, SW of Pangong and Shyok valleys, the strike of thrusts and the presence of vertical mineral lineation (Fig. 2C) is in agreement with a NNW–SSE shortening context.

4. Geochemical nature of Pangong Range metamorphic rocks

Amphibolite grade rocks have been sampled along the Pangong Range (LK96 series, Table 1) for major element geochemical analyses. The sample compositions are comprised between 52 and 63 wt% silica, with compositions similar to that of Shyok Suture Zone volcanic rocks (Fig. 4A), with relatively high Al_2O_3 (11.9–16 wt%) and low TiO_2 contents (0.4–1.3 wt%). Similarly to Shyok Suture Zone volcanics (Petterson and Windley, 1991; Treloar et al., 1996; Rolland et al., 2000, 2002a), a sub-linear decrease of TiO_2 contents with increasing SiO_2 can be observed, between 50 and 65 SiO_2 wt% (Fig. 4B). These features (high Al_2O_3 and low TiO_2) are commonly found in Calk-alkaline volcanic arc settings (e.g., Juteau and Maury, 1997; for a discussion of the arc affinity of Shyok samples see Rolland et al., 2000, 2002a).

5. Petrography and thermobarometry

5.1. Central granulitic core of the Pangong Massif

The central part of the Pangong Massif displays three types of granulitic assemblages (Table 2): clinopyroxene–pargasite–scapolite–spinel–quartz–plagioclase assemblage (Assemblage 1), orthoamphibole–garnet–spinel–rutile assemblage (Assemblage 2) and garnet–biotite–plagioclase–quartz (Assemblage 3).

5.1.1. P–T conditions of granulite facies

The presence of scapolite (Meionite variety) imposes high temperatures, above 800 °C (Goldsmith, 1976; Fig. 5 and Table 2). The jadeitic content of clinopyroxene (7%), in the presence of plagioclase, yields a pressure of 5.5 kbar at 800 °C (Fig. 6; Holland, 1980). The presence of rutile, equilibrated with a pyrope-rich garnet (X_{py} = 49.2, Table 2), implies minimal pressure of 5 kbar and temperature of 800 °C (Bohlen et al., 1983). A complementary *P–T* estimate, using the Thermocalc software on the assemblage 2, yields a similar result of $T = 870 \pm 70$ °C and $P = 7.1 \pm 1.2$ kbar for the temperature peak.

5.1.2. P–T conditions of amphibolite facies

The granulites were retromorphosed under amphibolite facies conditions by crystallisation of hornblende, garnet and biotite (Fig. 5). The presence of orthoamphiboles suggests an early retrogression due to shearing in granulite grade conditions (Dasgupta et al., 1999). Clinopyroxene to hornblende transformation indicates a thermal drop to 750–775 °C at a pressure of 4–8 kbar (Spear, 1981). The garnet–hornblende thermometer of Graham and Powell (1984) yields temperature estimates of 660–850 °C. A pressure estimate of 5 kbar at 700 °C is yielded by the Al con-

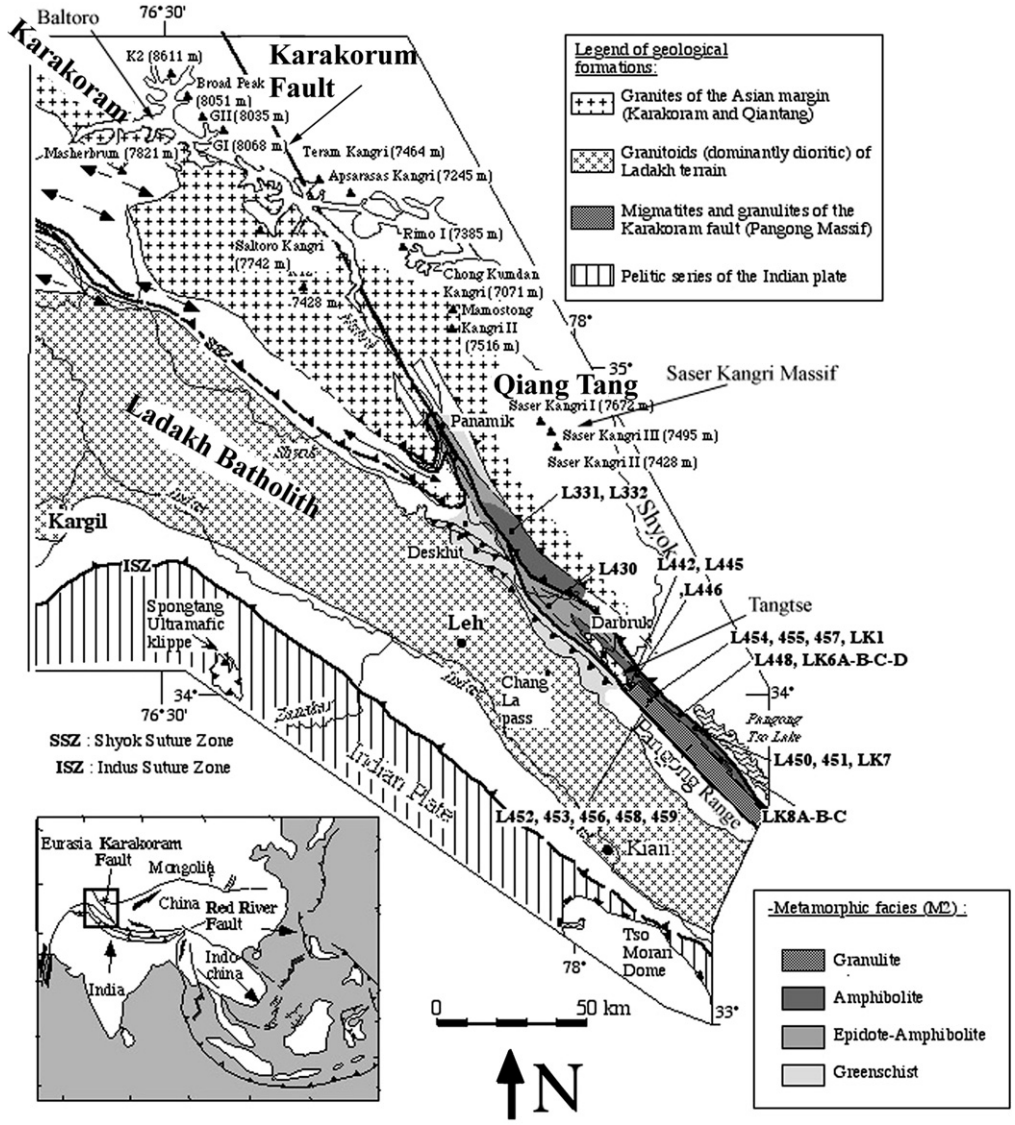

Fig. 1. Geological sketch map of the Karakorum Fault area in NW India. Insert, location and setting within the SE Asian tectonic context.

tent of hornblende of up to 2.9 p.f.u (Plyusnina, 1982). Similar estimates are obtained with Thermocalc for most samples (ranging from 500 ± 20 to 650 ± 40 °C), showing that the samples were strongly reequilibrated in the amphibolite facies during shearing.

5.1.3. LT retrogression

Increasingly more calcic compositions of amphibole from core (paragasite) to rim (actinolite), and garnet–biotite cationic exchange thermometry define retrogressive conditions in the lower amphibolite to upper greenschist facies (600–450 °C at P = 4 kbar). Finally, the crystallisation of actinolite–chlorite–albite assemblages in the zones of ductile–brittle reactivation defines further retrogression in the greenschist facies (Moody et al., 1983).

5.2. Pangong amphibolitic unit

The Eastern amphibolite facies part of Pangong Range consists mainly of metapelites, showing the assemblage biotite–plagioclase–muscovite–sillimanite–garnet–quartz (Assemblage 4). Muscovite, sillimanite, and biotite define the foliation.

The co-stability of muscovite and sillimanite, in absence of K-feldspar, defines temperatures between 650 and 730 °C at 7 kbar (Hodges and Spear, 1982; Le Breton and Thompson, 1988; Vielzeuf and Holloway, 1988). P–T estimates based on cationic exchange thermobarometers yield conditions of T = 700 ± 20 °C (Fig. 7; Ferry and Spear, 1978; Ganguly and Saxena, 1984; Hodges and Spear, 1982) and P = 7 ± 1 kbar (Ghent and Stout, 1981; Hodges and Crowley, 1985; Hoisch, 1990; Plyusnina, 1982).

5.3. Saser Kangri metamorphic rocks

NE to the Nubra valley and Karakorum Fault, the Saser Kangri metamorphic rocks consist of metapelites bearing the assemblage: andalusite–cordierite–biotite–albite–quartz ± sillimanite ± garnet. This assemblage features low pressure amphibolite conditions. Using the X_{Mg} (0.58, Table 2) content of cordierite, in presence of garnet, the metamorphic peak can be fixed at a pressure of

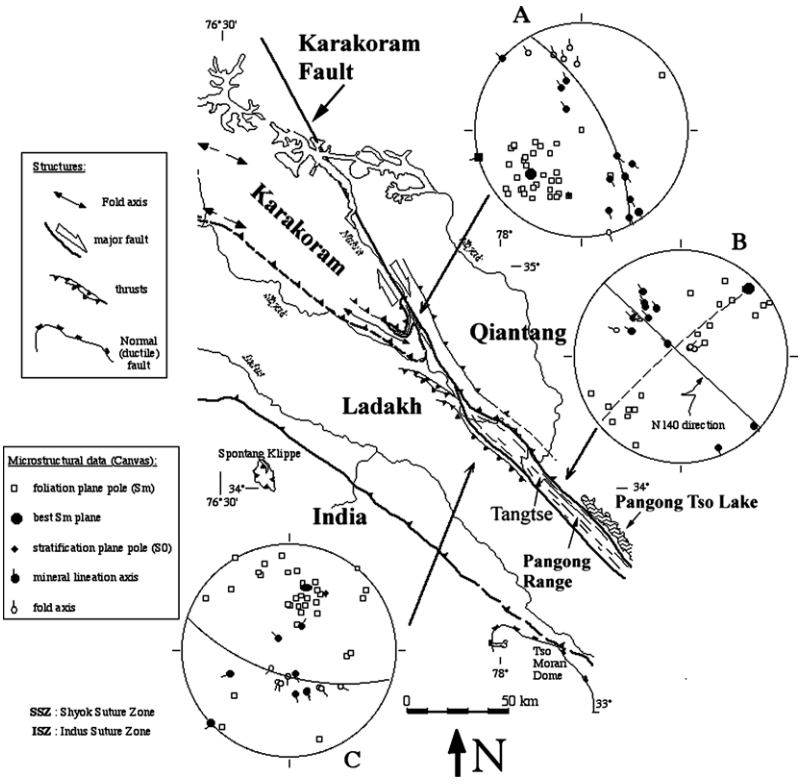

Fig. 2. Simplified structural map of the Karakorum Fault (N-Ladakh, India), with microstructural data plots (Wulff canvas plots in lower hemisphere).

5.5 ± 1 kbar at a temperature of 660 ± 50 °C (Fig. 7), according to the barometer of Vielzeuf (1984).

6. Age of HT metamorphism

Two samples, from the amphibolitic and granulitic units of the Pangong Range, have been selected for Ar analysis. The Ar data are displayed on Table 3 and Fig. 8.

The Ar systematics of sample L441 are simple (c, Fig. 8). The Ca/K ratio is uniform in steps 2–6, which account for >90% of the Ar release. Similarly, in these steps the Ca/Cl ratio varies only between 76 and 101. This small chemical variation suggests that there is essentially only one amphibole generation, and accordingly its step ages are uniform and average 13.6 ± 0.9 Ma (2σ). Both these features suggest that the amphibole was completely crystallized during the amphibolite facies shearing event.

The Ar spectrum of sample L450 (a, Fig. 8) shows a staircase shape, with step ages ranging from 18.6 ± 0.8 to 30.6 ± 0.8 Ma. In steps 3–8, which account for 87% of the Ar release, Ca/K ratios are very uniform between 32.6 and 33.4, but Ca/Cl ratios vary significantly between 1174 and 1425 defining a good correlation with age. This information suggests that a young, Cl-rich amphibole overgrew an old, Cl-poor one, but in order to achieve a conclusive proof it would be necessary to acquire additional electron microprobe data. With microchemical and microstructural data, it is possible to reliably date successive amphibole generations (Villa et al., 2000). As a further example of the method's potential, we recall the distinction between ages of granulitic amphibole cores and amphibolite-facies rims on the basis of correlated Al^{IV}/Al^{VI} and Ca/K ratios (Villa et al., 1996) or on the basis of correlated Ca/Cl and Ca/Al ratios (Kreissig et al., 2001).

For pargasite L450, four electron microprobe analyses along a core–rim traverse were acquired. They show a uniform increase of the Ca/K ratio between cores (Ca/K = 25.3) and rims (Ca/K = 34.7). However, the Al^{IV}/Al^{VI} ratios are constant, which requires that cores and rims were formed at the same *P–T* conditions, presumably in a very short time. On the other hand, the Ca/K ratio of the gas-rich steps is uniform, which may reflect the fact that during hand-picking the transparent rims were efficiently purified at the expense of more inclusion-rich cores. Any interpretation of step ages up to 30 Ma is, therefore, highly speculative and will not be pursued here. In conclusion, our two amphibole ages appear to bracket the 18.0 ± 0.6 Ma emplacement of Tangtse granite (U–Pb on zircon, Searle et al., 1998).

7. Discussion

Several questions remain to be solved, concerning the tectono-metamorphic evolution of the Karakorum–Tibet boundary. What is the importance of the Karakorum Fault, including the depth, total offset and age of initiation of this fault? What is the reason for the HT metamorphic evolution observed in both the Karakorum margin and the Karakorum Fault?

7.1. Depth of the Karakorum Fault

The above *P–T* estimates give some constrains to the *P–T* path followed by the granulitic core of the Pangong Range and its eastern amphibolitic slice (Fig. 9). The *P–T* path of the granulitic core is characterised by a strong decrease in temperature from 18 km depth (pressure of 6 kbar). The *P–T* path of the amphibolitic slice becomes similar to the granulitic unit at ~12 km (4 kbar). These data suggest that an anomalous thermal flux is present at shallow levels in the fault zone (50 °C km^{-1} at 10 km depth). Such anomalous thermal gradient has also been observed in current and fossil major strike-slip faults, such as the Red River fault zone (Leloup

Please cite this article in press as: Rolland, Y. et al., Syn-kinematic emplacement of the Pangong metamorphic and magmatic complex along the Karakorum Fault (N Ladakh) ..., Journal of Asian Earth Sciences (2008), doi:10.1016/j.jseaes.2008.03.009

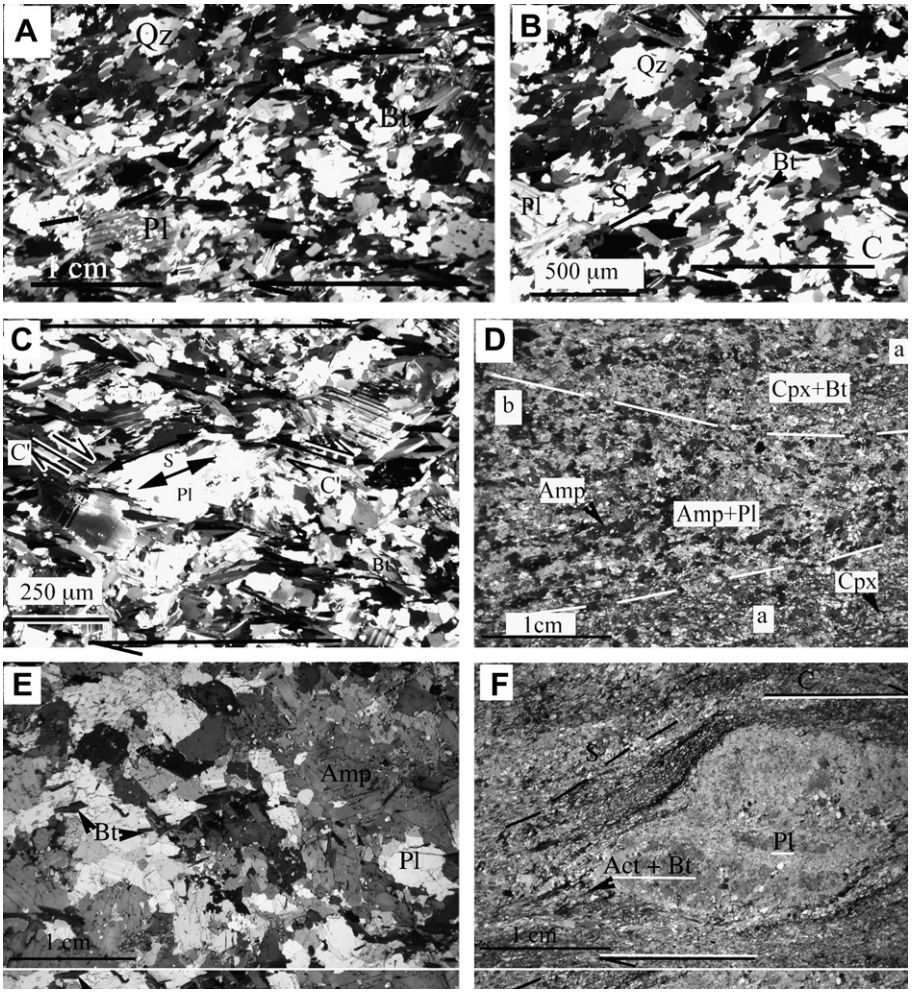

Fig. 3. Micro-photographs of microstructures and lithologies. (A–C) The Tangtse granite in crossed polars (sample L445, X-Z N140°E horizontal section). The texture is shown at centimetre (A) to millimetre (C) scales. Dextral sense of shear is deduced from the curvate schistosity (S) and shear planes parallel (C) or oblique at 30–40°(C′) with respect to the picture N140°E orientation. Also note that the orientation of porphyritic feldspar crystals, as well as biotite is acquired previously to the crystallisation of quartz that "seals" the syn-magmatic fabric. Strike-slip shearing necessarily occurred before the complete crystallisation of the granite. (D) Granulite-grade sample (L452) showing cpx-bearing lenses (a) separated by zones of amphibolitized (hornblende bearing) rock (b). (E) Porphyritic amphibolite (sample L441) showing large granular amphibole (hornblende) crystals. (F) Greenschist facies rock (sample L457), with deformed plagioclase porphyroclasts suggesting a volcanic andesitic basalt protolith; the sense of shear is clearly dextral as shown by the C–S relationships.

and Kienast, 1993) in SE Asia, and in the Great Slave shear zone in Canada (Hoffman, 1987; Hanmer, 1988). These HT gradients have firstly been interpreted as the result of shear heating (Leloup and Kienast, 1993; Leloup et al., 1995). However, the estimated gradient in the Karakorum Fault is higher (ΔT, Fig. 9) or similar to the highest estimates modelled for a single shear heating process alone (30 °C km^{-1}; Leloup et al., 1999; Nabelek et al., 2001). This high thermal gradient, i.e., raising isotherms, could be due to heat advection (by magmatic ascent) and conduction along the fault zone. Mantle-derived magmas (lamprophyres and syenites) are known in the Karakorum Fault region NE of K2 (Pognante, 1990), and within the Karakorum metamorphic Complex where they are dated at 20–22 Ma by whole-rock K–Ar ages (Rex et al., 1988). Their mantle origin is shown by their mineralogy and geochemistry composition (Pognante, 1990; Rex et al., 1988; Mahéo et al., 2002). Such magmas could thus provide significant heat imput and confirm that the Karakorum Fault could be a crustal to lithosphere-scale shear zone (Fig. 10), as previously proposed for the Red River Fault (Leloup et al., 1999) and the Altyn Tagh Fault (Wittlinger et al., 1998).

7.2. Exhumation of the Pangong Massif

The Tangtse granite, which has been intruded in the amphibolitic unit at the contact with the granulitic core unit, has been dated at 18 Ma (U/Pb on zircon) by Searle et al. (1999). As metamorphic conditions reached in the amphibolitic unit were just below the muscovite dehydration melting reaction (Le Breton and Thompson, 1988; Vielzeuf and Holloway, 1988), a rather small thermal increase at the contact with the granulitic unit could have been sufficient to trigger partial melting. If we accept this interpretation, the 18 Ma age of the Tangtse granite dates the muscovite dehydration melting reaction in the amphibolites. The concordant 18 Ma Ar–Ar age component in granulite sample L450 suggests that the age of 18 Ma could also correspond to the tectonic stacking of the two units. The Ar–Ar hornblende crystallization at13.6 ± 0.9 Ma would date further amphibolite-facies shearing at 600 ± 50 °C. Further cooling down to 500 °C (e.g., Di Vincenzo et al., 2003) is dated at ca. 11 Ma by Ar–Ar data of Tangtse granite muscovite obtained by Searle et al. (1999).

Please cite this article in press as: Rolland, Y. et al., Syn-kinematic emplacement of the Pangong metamorphic and magmatic complex along the Karakorum Fault (N Ladakh) ..., Journal of Asian Earth Sciences (2008), doi:10.1016/j.jseaes.2008.03.009

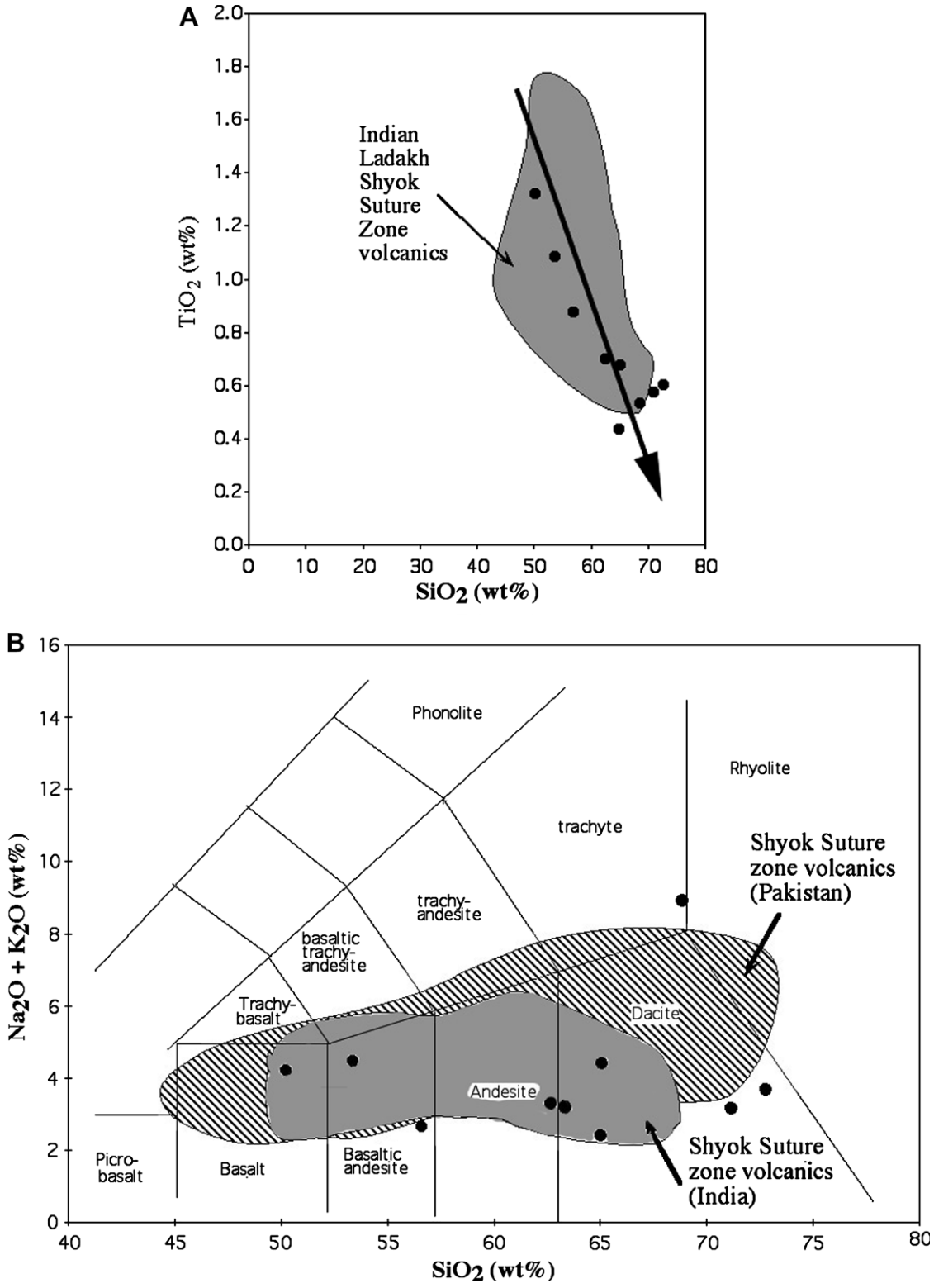

Fig. 4. (A) Na_2O+K_2O vs. SiO_2 plot of Pangong Massif metamorphic rocks. (B) TiO_2 vs. SiO_2 plot of Pangong Range rocks. Note that the values obtained for Pangong Range rocks plot within the field of Ladakh Shyok Suture Zone volcanic rocks [data from Rolland et al. (2000, 2002)].

These age estimates allow *P–T–t* path reconstitution for the Pangong Range (Fig. 10), and derivation of vertical exhumation rates for the Pangong Massif, albeit still imprecise. Transition from Tangtse granite emplacement (zircon age, 18 Ma) to amphibolite-facies shearing (Ar amphibole age, 13.6 ± 0.9 Ma), for which in Section 5 we provided a temperature window between ca. 500 and 650 °C and $P = 4$ kbar, corresponds to a pressure decrease of ca. 1 kbar, or 3 ± 1 km. Thus, the vertical exhumation rate of the Pangong Range can be estimated to 0.7 ± 0.2 mm a^{-1}. The white mica ages (Searle et al., 1999) pertain

Please cite this article in press as: Rolland, Y. et al., Syn-kinematic emplacement of the Pangong metamorphic and magmatic complex along the Karakorum Fault (N Ladakh) ..., Journal of Asian Earth Sciences (2008), doi:10.1016/j.jseaes.2008.03.009

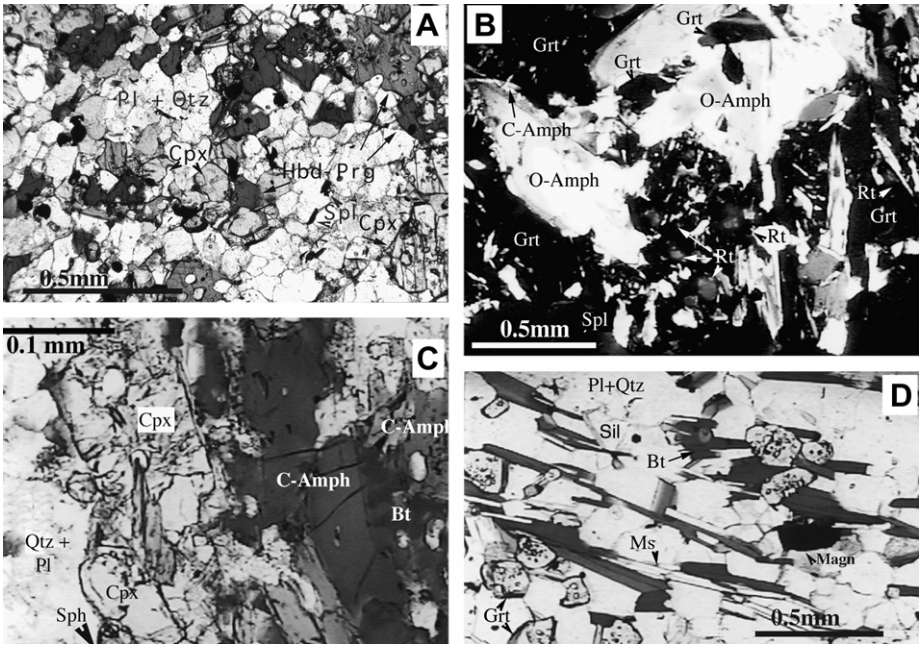

Fig. 5. Granulite and amphibolite grade assemblages photographs (A, B, D in natural light and C in polarised light). (A) Clinopyroxene grains mantled by hornblende (C-Amph) and biotite (sample L441); (B) microgranular texture made of clinopyroxene–amphibole (hornblende–pargasite; sample L448)–plagioclase–quartz–spinel; (C) large and zoned acicular to prismatic orthoamphibole grains (O-Amph), of anthophyllite to gedrite compositions, locally fringed by hornblende (C-Amph; sample L456). Orthoamphibole crystals nucleated around rutile grains, and are included in cm-large poekilitic garnet that constitutes the opaque background of the picture. (D) Amphibolite-grade metapelite (E-Pangong, sample L446), showing a biotite–garnet–muscovite–quartz–plagioclase–sillimanite assemblage.

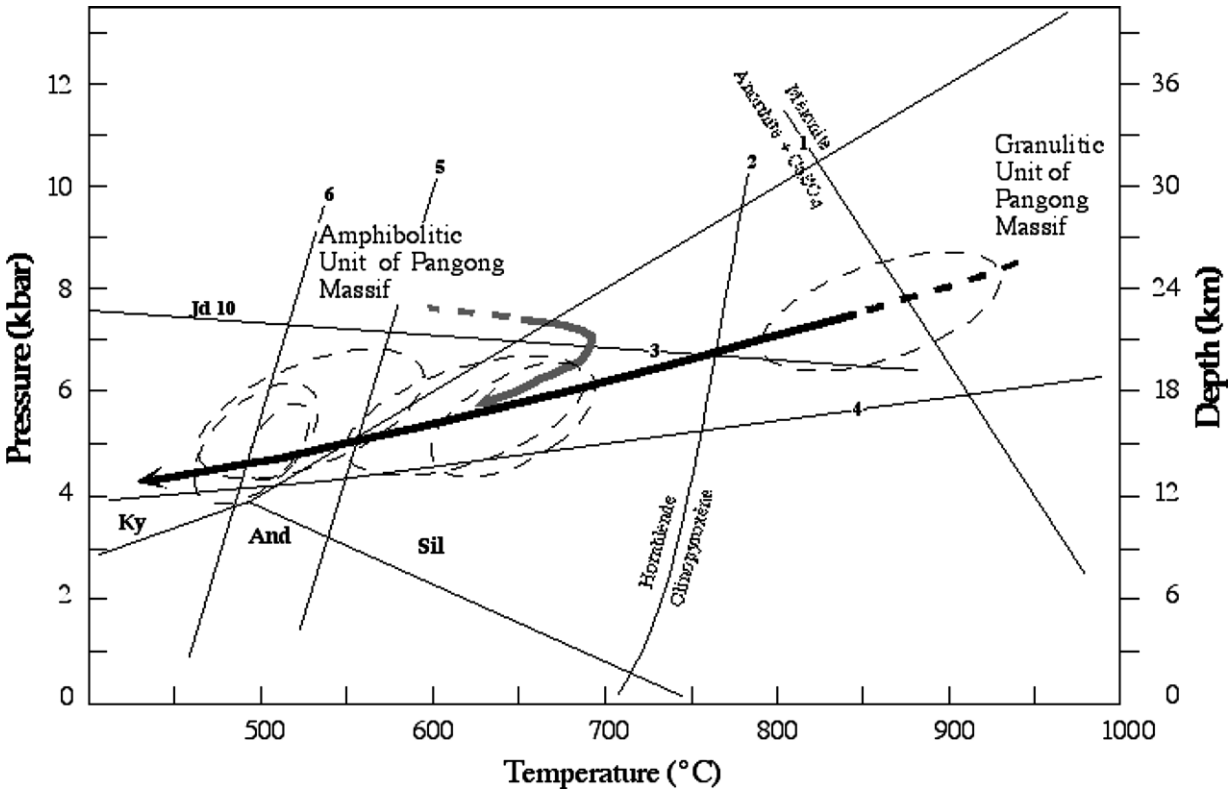

Fig. 6. *P–T* path of metabasites from the Pangong Massif granulitic unit (CaFMASH system). (1) from Goldsmith (1976); (2) from Spear (1981); (3): Albite = Jadeite + Quartz, after Holland (1980); (4): Garnet (Xalm: 0.4) + Rutile = Ilmenite + Aluminosilicate + Quartz, after Bohlen et al. (1983); (5) Albite + Chlorite + Epidote + Actinolite = Plagioclase + Hornblende, after Schiffman and Liou (1980); (6) Chlorite + Epidote + Quartz = Tschermakite + Anorthite + H_2O, after Nitsch (1971). Thermocalc *P–T* estimates are shown by ellipses (2σ error).

Please cite this article in press as: Rolland, Y. et al., Syn-kinematic emplacement of the Pangong metamorphic and magmatic complex along the Karakorum Fault (N Ladakh) ..., Journal of Asian Earth Sciences (2008), doi:10.1016/j.jseaes.2008.03.009

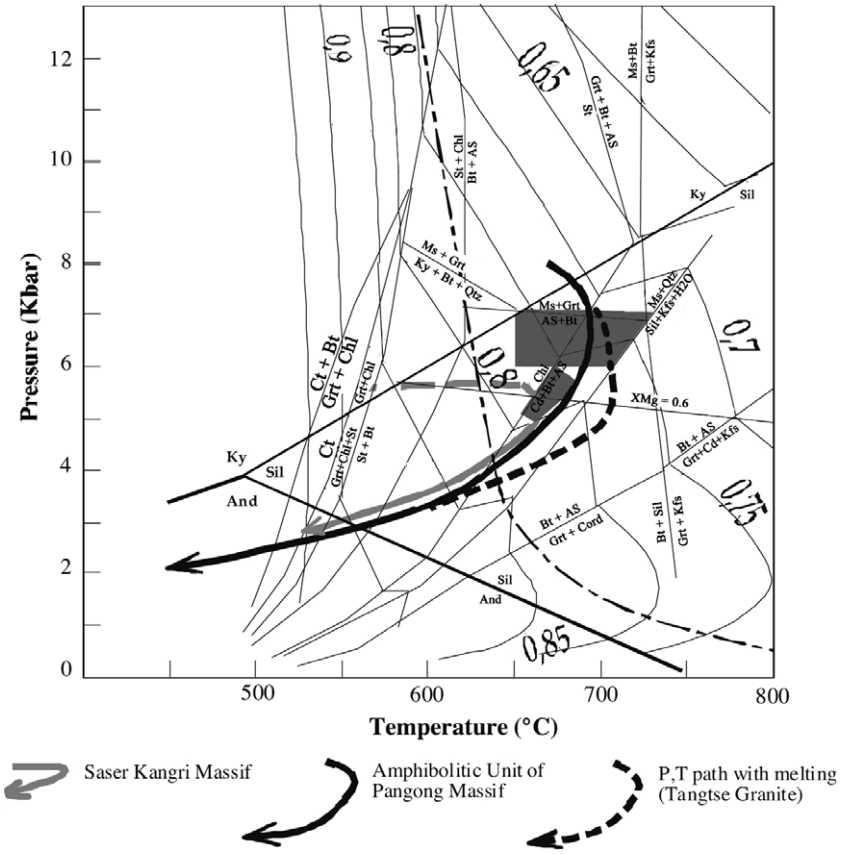

Fig. 7. *P–T* paths for the metapelites of the different units of the studied area (KFMASH system), $X_{H2O} = 1$ and quartz in excess. Dotted lines are almandine isopleths. The H_2O-saturated metapelite solidus is after Thompson (1982); Grt + Ms and Grt + Kfs producing reactions are from Vielzeuf (1984) and Vielzeuf and Holloway (1988); Ms to Kfs + Sil destabilisation from Le Breton and Thompson (1988). $X_{Mg} = 0.6$ isopleth of cordierite after Vielzeuf (1984). Other reactions are from Spear and Cheney (1989). Minerals abbreviations following Kretz (1983).

to the cessation of cation exchange, recorded by the garnet–biotite geothermometer, and thus to a similar temperature range of 600–450 °C (Section 5) and do not add precise constraints. From 18 Ma, the total vertical offset of the Pangong Range is estimated at 18 ± 1.5 km. Thus, the most robust estimate is the average exhumation rate between 18 Ma and present is estimated at 1.0 ± 0.2 mm a^{-1}. We note that it is three times lower than in some areas of the Karakorum Metamorphic Complex of Pakistan (Dassu Dome: 3 mm a^{-1}, Rolland et al., 2001, 2006a). A horizontal offset can be estimated from the 18 km exhumation using the 30° plunge of lineations in the Pangong Range: the horizontal offset is calculated as 31 ± 3 km. This offset corresponds to the time between 18 Ma and present.

7.3. Geological offsets of the Karakorum Fault

Searle et al. (1998) have estimated a c. 150 km offset from the correlation of the Baltoro Batholith with the Tangtse granite. This correlation appears to be unlikely because (1) the Tangtse granite has been dated at 18 Ma, diachronous to the Baltoro Batholith, dated between 25 and 21.5 Ma (Parrish and Tirrul, 1989; Schärer et al., 1990a). Further, the Baltoro and Tangtse granites are dissimilar considering both emplacement mode and volume. The Baltoro Batholith has emplaced as a great sill within the Karakorum series, while Tangtse granite is a complex dyke network emplaced synkinematically within the fault zone during dextral motion. Consequently, the Tangtse granite is not offset by the active Karakorum fault and therefore cannot be used to estimate the amount of vertical offset along this fault. Moreover, as shown by the geochemical analyses, the Pangong Range amphibolites bear volcanic arc features similar to Shyok Suture Zone volcanic rocks and are unlikely to be correlated to the Karakorum series, which are mostly formed by interlayered metapelites and marble series (Rolland et al., 2002b, 2006a). Tangtse granite exhibits zoned zircons, with inherited core U–Pb ages of 106 Ma (Searle et al., 1999), overgrown by magmatic zircon with ages of 18 Ma. The inherited zircon age of the Tangse granite is within the range of the paleontological and radiometric age of Shyok Suture Zone formations (Aptian–Albian; Rolland et al., 2000, 2006b), which is in agreement with the Shyok volcanics being a source for the Tangtse Granite. In contrast, the Baltoro granite zircon shows Precambrian inheritance (Parrish and Tirrul, 1989), and is therefore unlikely correlated with the Tangtse Granite. The Karakorum Fault offsets could rather be deduced from the correlation of geological terrain accreted to the Asian margin. Cambro–Ordovician rocks are observed all along the S–Karakorum margin, (LeFort et al., 1994; Rolland et al., 2002b). Such Cambro–Ordovician successions of rocks have also been found in the Lhasa block. There, Xu et al. (1985) have described early Cambrian basement gneiss (539 ± 14 Ma), and unmetamorphosed Ordovician sediments overlie this basement (Yin et al., 1988). Further, both Lhasa and Karakorum terrains were accreted in the Upper Jurassic–Lower Cretaceous period (Zanchi et al., 2000). The correlation of the Karakorum and Lhasa blocks based on the current positions of the Kilik fault, northern boundary of Karakorum (Gaetani et al., 1990a,b) and of the Bangong suture (northern boundary of the Lhasa block) suggests a total offset of

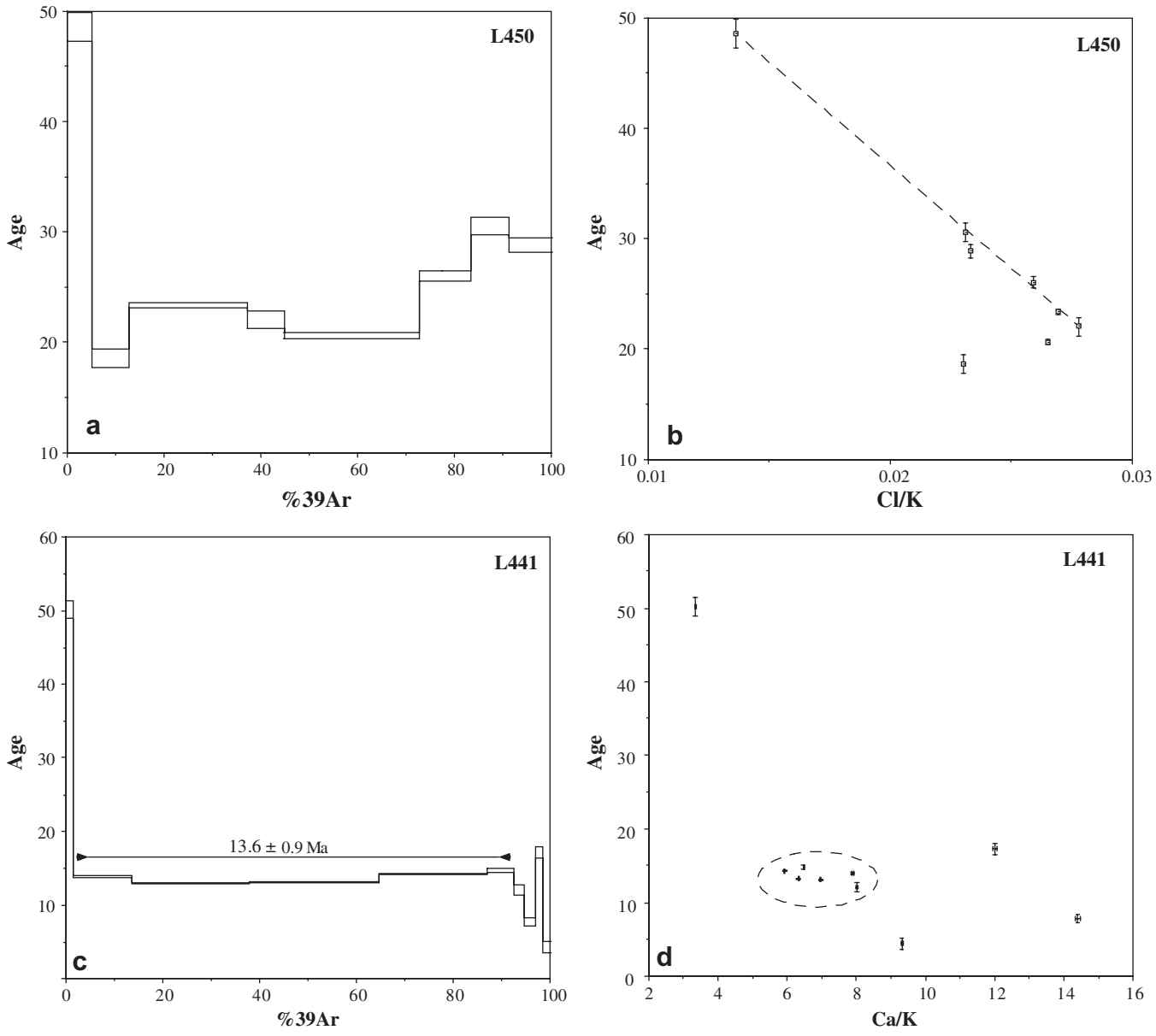

Fig. 8. $^{40}Ar/^{39}Ar$ stepwise heating data plots for samples L441 (granulite) and L450 (amphibolite).

~300 km along the central part of the Karakorum Fault. This estimate is comparable to the estimate made by Lacassin et al. (2004a,b) based on the correlation of Shyok and Shiquanhe suture zones (Fig. 11).

7.4. Age of initiation and slip rates of the KF

Metamorphic rocks are clearly syn-kinematic as shown by mineral growth in the direction of the mineral/stretching lineation within the fault zone. Then, the oldest metamorphic age (that of the temperature peak of the Pangong Range) is a minimum age for the initiation of slip along the KF. The HT event is microstructurally contiguous to the amphibolite facies retrogression, and would therefore be predicted to be temporally quite close, because relaxation of the thermal anomaly of 700 °C at 5–6 kbar would last less than 1 Ma. For a HT age of 18 Ma, the slip rate is ca. 17 mm a^{-1}. On the other hand, granulite facies metamorphism could be coeval with U–Pb age of 32 ± 3 Ma obtained on syn-metamorphic and syn-kinematic leucogranites on other portions of the KF (Valli et al., 2003), and on leucogranites of the Pangong Range itself (Searle et al., 1998). Taking into account this 32 Ma age, and the estimated 300 km of offset, the mean slip rate of the Karakorum Fault would be a minimum of ca. 10 mm a^{-1}. Such value is similar with Quaternary rate estimates based on cosmogenic dating of offset moraines (10.7 ± 0.7 mm a^{-1}, Chevalier et al., 2005). The initiation of the Karakorum Fault would then be sub-contemporaneous to that of the Red River Fault (30–40 Ma, Lacassin et al., 1997). The metamorphic evolution of the Pangong Range appears to be quite similar considering *P–T* evolution to that of the Red River fault. Similar U–Pb and Ar–Ar ages were obtained in both the Karakorum and Red River faults (Tapponnier et al., 1990; Harrison et al., 1992; Leloup et al., 1995; Lacassin et al., 1997; Schärer et al., 1990b, 1994), suggesting that these two faults have acted as comparable boundaries of the extruding Tibetan bloc during the Miocene

Please cite this article in press as: Rolland, Y. et al., Syn-kinematic emplacement of the Pangong metamorphic and magmatic complex along the Karakorum Fault (N Ladakh) ..., Journal of Asian Earth Sciences (2008), doi:10.1016/j.jseaes.2008.03.009

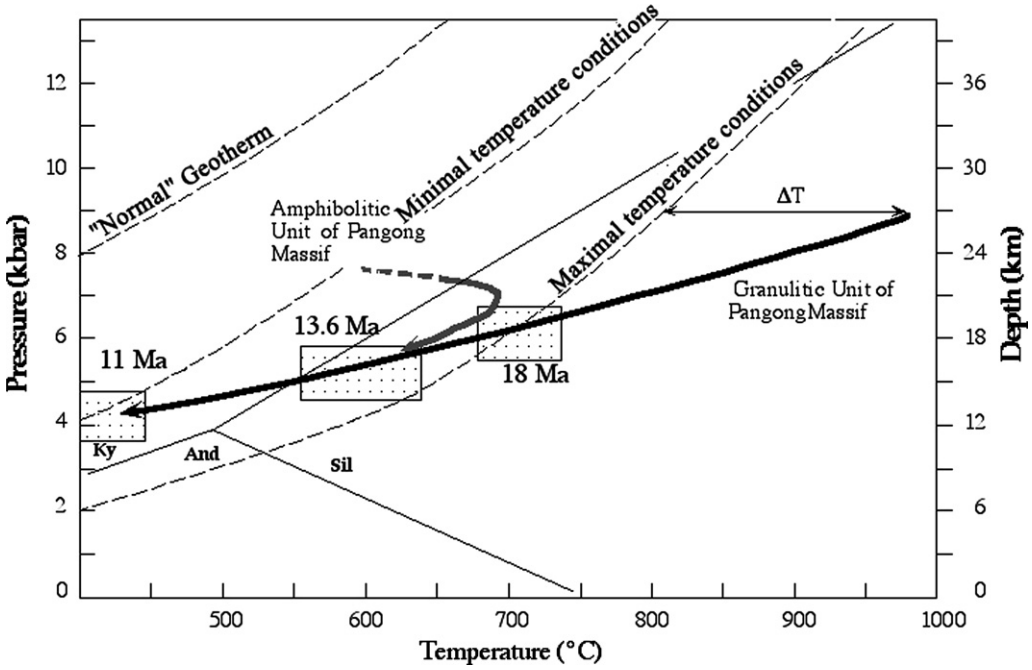

Fig. 9. Pressure–Temperature–time paths obtained for Pangong granulites and amphibolites. The broken lines represent (from left to right): 1, "normal" geothermal conditions prevailing in an unperturbed lithosphere; 2–3, modelled conditions of minimal and maximal heat input by shear heating in a crustal-scale shear zone (Leloup et al., 1999). Minerals abbreviations following Kretz (1983).

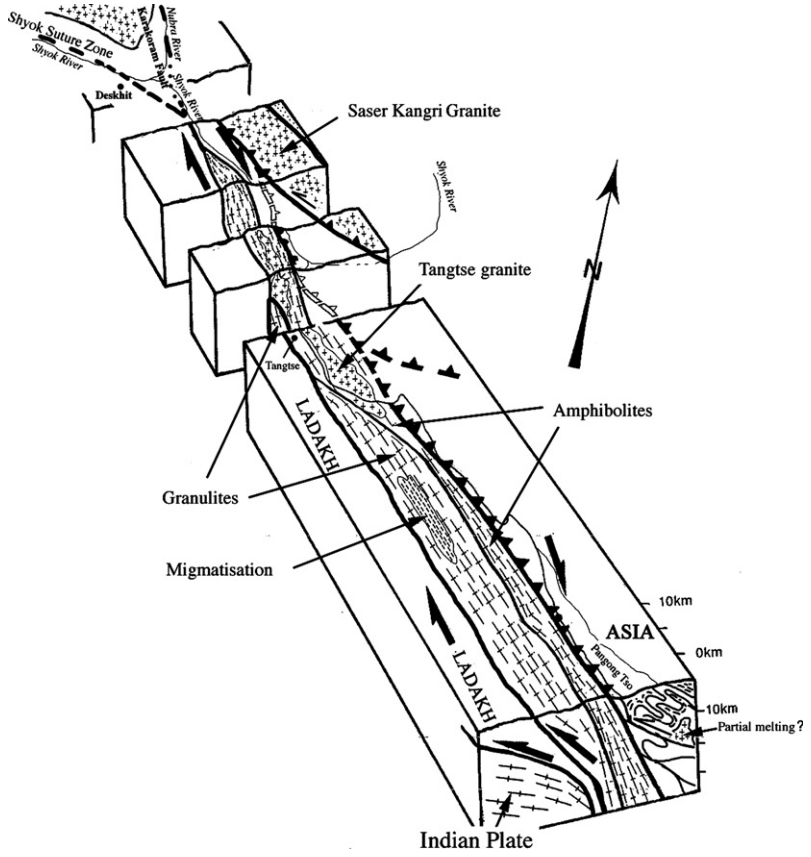

Fig. 10. Schematic 3D interpretative view of the Karakorum Fault structure along Nubra, Shyok and Pangong valleys.

Please cite this article in press as: Rolland, Y. et al., Syn-kinematic emplacement of the Pangong metamorphic and magmatic complex along the Karakorum Fault (N Ladakh) ..., Journal of Asian Earth Sciences (2008), doi:10.1016/j.jseaes.2008.03.009

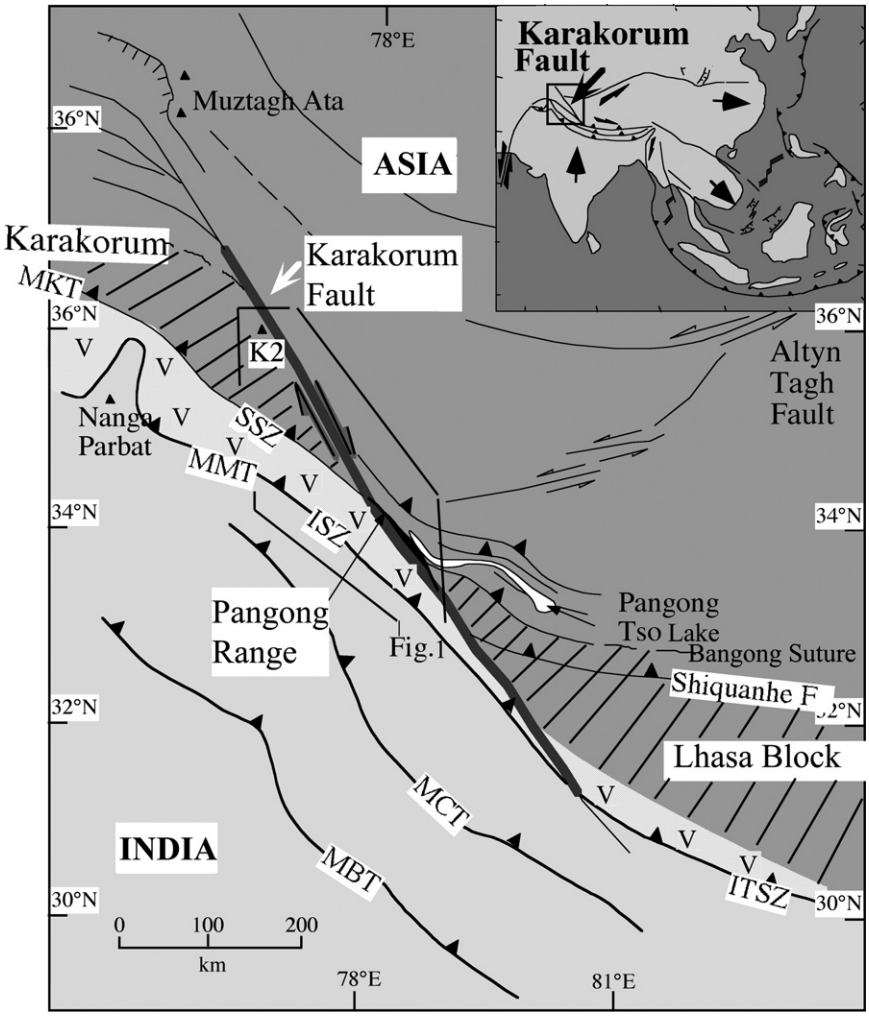

Fig. 11. Sketch geological map of the Karakorum Fault, showing in particular the offset of the Karakorum Fault if a correlation of Karakorum and Lhassa terrains is done.

(Burdigalian). In the light of deformation pattern observed in the S-Karakorum region (Fig. 12; Rolland et al., 2002a; Mahéo et al., 2004), the lateral extrusion of Tibet could be also accommodated by ductile flattening (vertical folding) within the Karakorum and Tibet terrains, due to the rheology of the granulitic grade mid-crustal levels (e.g., Le Pichon et al., 1997; Burg and Podladchikov, 1999).

8. Conclusion

1. The thermal evolution of the Karakorum Fault has been studied in the Pangong Range area. The thermobarometric estimates point out HT rocks, equilibrated at $T > 800$ °C, $P = 5.5$ kbar. These rocks successively, and partially, reequilibrated in the amphibolite facies at 700–750 °C, 4–5 kbar, and in the greenschist facies.

2. Syn-magmatic C–S structures observed within the Tangtse granite show very clearly that this granite was emplaced syn-kinematically within the KF, and not offset by the KF as previously suggested.

3. Compiled U–Pb zircon, Ar–Ar mica and additional Ar–Ar amphibole age give further constrains on the *P*, *T*, *t* path of the Pangong Range. Amphibolitisation at 700–750 °C is constrained by the Tangtse granite emplacement at 18 Ma (U/Pb zircon). A similar age range is suggested by incomplete Ar–Ar resetting of amphibole sample L450. Deformation continued to lower temperatures of ca. 650–500 °C at least until 13.6 ± 0.9 Ma (Ar–Ar amphibole age of sample L441). Post-deformation greenschist-facies muscovite grew at 11 Ma.

4. The HT conditions observed in the Pangong Range reveal a very high thermal gradient within the fault. This gradient lies at higher temperature conditions than the conditions modelled for a simple shear heating process within a trans-Lithospheric fault, suggesting that additional heat advection within the fault is to be advocated.

5. Correlating the Karakorum and Lhasa terrains, which are formed by similar Cambro–Ordovician series and accreted subcontemporaneously to the Asian margin, we propose a total offset of 300 km since the collision at the Upper Jurassic–Lower Cretaceous transition.

6. Finally, the observed tectonic and metamorphic evolutions at the Karakorum–Tibet boundary may be the result of crustal-scale partitioning between strike-slip faulting, along the Karakorum Fault, and folding within the Karakorum margin (Fig. 12). In this context, HT metamorphism observed and mantle-derived magmatism are interpreted to result from a slab detachment process.

Acknowledgements

Field work and laboratory analyses were financially supported by LGCA-UMR 5025. Within the LGCA, we particularly thank H. Lapierre, G. Mascle and S. Guillot for discussions and F. Senebier

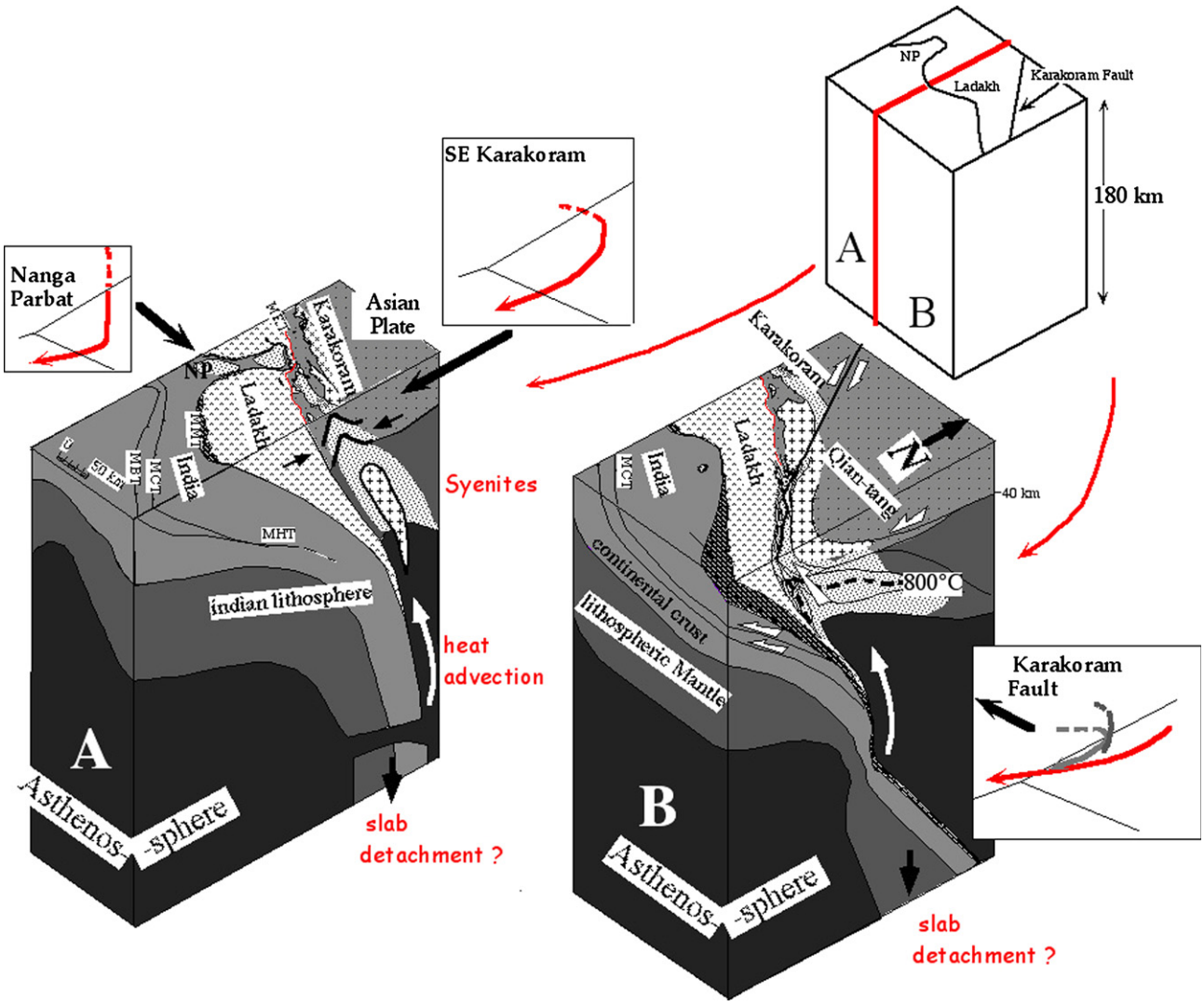

Fig. 12. 3D sketch of the Karakorum–Tibet corner. (A) Pakistan NW syntaxis and (B) Karakoram Fault zone, with the *P–T* paths obtained in each area. Nanga Parbat *P–T* path from Zeitler et al. (1993); SE Karakoram *P–T* path from Rolland et al. (2001, 2006a); Karakoram Fault, this study. Asthenosphere uprise is interpreted as the result of a slab detachment process.

is thanked for the separation of amphiboles. The authors wish to thank P. Treloar, H. Martin and J.M. Lardeaux for discussions. We are also grateful to M. Oddone for his collaboration for amphibole irradiation, to P. Capiez for the acquisition of major element data and to M. Veschambre for her help in providing electron microprobe data.

References

Armijo, R., Tapponnier, P., Han, Tonglin, 1989. Late Cenozoic right-lateral strike-slip faulting across southern Tibet. Journal of Geophysical Research 94, 2787–2838.

Berthé, D., Choukroune, P., Jegouzo, P., 1979. Orthogneiss, mylonite and non coaxial deformation of granites: the example of the South Armorican shear zone. Journal of Structural Geology 1, 31–42.

Bohlen, S.R., Wall, V.J., Boettcher, A.L., 1983. Experimental investigations and geological applications of equilibria in the system FeO–TiO_2–Al_2O_3–SiO_2–H_2O. American Mineralogist 68, 1049–1058.

Burg, J.P., Podladchikov, Y., 1999. Lithospheric scale folding: numerical modelling and application to the Himalayan syntaxes. International Journal of Earth Sciences 88, 190–200.

Chevalier, M.L., Ryerson, F., Tapponnier, P., Finkel, R., Van Der Woerd, J., Haibing, L., Liu, Q., 2005. Slip-rate measurements on the Karakorum Fault may imply secular variations in fault motion. Science 307, 411–414.

Dasgupta, S., Sengupta, P., Sengupta, P., Ehl, J., Raith, M., 1999. Petrology of gedrite–bearing rocks in mid-crustal shear zones of the Eastern Ghats Belt, India. Journal of Metamorphic Geology 17, 765–778.

Di Vincenzo, G., Carosi, R., Palmeri, R., 2003. The relationship between tectono-metamorphic evolution and argon isotope records in white mica: constraints from in situ ^{40}Ar–^{39}Ar laser analysis of the Variscan basement of Sardinia (Italy). Journal of Petrology 45, 1013–1043.

Ferry, J.M., Spear, F.S., 1978. Experimental calibration of the partitioning between biotite and garnet. Contributions to Mineralogy and Petrology 66, 113–117.

Gaetani, M., Garzanti, E., Jadoul, F., Nicora, A., Tintori, A., Pasini, M., Ali Khan, K.S., 1990a. The north Karakorum side of the Central Asia geopuzzle. Geological Society of America 102, 54–62.

Gaetani, M., Gosso, G., Pognante, U., 1990b. A geological transect from Kun Lun to Karakorum (Sinkiang, China): the western termination of the Tibetan Plateau, Preliminary note. Terra Nova 2, 23–30.

Ganguly, J., Saxena, S.K., 1984. Mixing properties of aluminosilicate garnets: constraints from natural and experimental data, and applications to geothermo-barometry. American Mineralogist 69, 88–97.

Ghent, E.D., Stout, M.Z., 1981. Geobarometry and geothermometry of plagioclase–biotite–garnet–muscovite assemblages. Contributions to Mineralogy and Petrology 76, 92–97.

Goldsmith, J.R., 1976. Scapolites, granulites, and volatiles in the lower crust. Geological Society of America Bulletin 87, 161–168.

Graham, C.M., Powell, R., 1984. A garnet–hornblende geothermometer: calibration, testing, and application to the Pelona Schist, Southern California. Journal of Metamorphic Geology 2, 13–21.

Hanmer, S., 1988. Great Slave Lake shear zone, Canadian shield: reconstructed vertical profile of a crustal-scale fault zone. Tectonophysics 149, 245–264.

Harrison, T.M., Chen, Wenji, Leloup, P.H., Ryerson, F.J., Tapponnier, P., 1992. An early Miocene transition in deformation regime within the Red River fault zone, Yunnan, and its significance for Indo-Asian tectonics. Journal of Geophysical Research 97, 7159–7182.

Hodges, K., Spear, F.S., 1982. Geothermometry, geobarometry and the Al_2SiO_5 triple point at Mt. Moosilauke, New Hampshire. American Mineralogist 67, 1118–1134.

Hodges, K., Crowley, P.D., 1985. Error estimation and empirical geothermobarometry for pelitic systems. American Mineralogist 70, 702–709.

Hoffman, P.F., 1987. Continental transform tectonics, Great Slave Lake shear zone (ca. 1.9 Ga), northwest Canada. Geology 15, 785–788.

Hoisch, T.D., 1990. Empirical calibration of six geobarometers for the mineral assemblage quartz + muscovite + biotite + plagioclase + garnet. Contributions to Mineralogy and Petrology 104, 225–234.

Holland, T.J.B., 1980. The reaction albite = jadeite + quartz determined experimentally in the range 600–120 °C. American Mineralogist 65, 129–134.

Holland, T.J.B., Powell, R., 1990. An enlarged and updated internally consistent thermodynamic dataset with uncertainties and correlations: the system K_2O–Na_2O–CaO–MgO–MnO–FeO–Fe_2O_3–Al_2O_3–TiO_2–SiO_2–C–H_2–O_2. Journal of Metamorphic Geology 8, 89–124.

Juteau, T., Maury, R., 1997. Géologie de la croûte océanique. Masson, Paris.

Kretz, R., 1983. Symbols for rock-forming minerals. American Mineralogist 68, 277–279.

Kreissig, K., Holzer, L., Frei, R., Villa, I.M., Kramers, J.D., Kröner, A., Smit, C.A., van Reenen, D.D., 2001. Age of early deformation of the Hout River Shear Zone and the metamorphism in the Southern Marginal Zone of the Limpopo Belt, Southern Africa. Precambrian Research 109, 145–173.

Lacassin, R., Maluski, H., Leloup, P.H., Tapponnier, P., Hinthong, C., Siribhakdi, K., Chuaviroj, S., Charoenravat, A., 1997. Tertiary diachronic extrusion and deformation of western Indochina: structural and $^{40}Ar/^{39}Ar$ evidence from NW Thailand. Journal of Geophysical Research 102, 10023–10037.

Lacassin, R., Valli, F., Arnaud, N., Leloup, P.H., Paquette, J.L., Li, H.B., Tapponnier, P., Chevalier, M.L., Guillot, S., Maheo, G., Xu, Z.Q., 2004. Large-scale geometry, offset and kinematic evolution of the Karakorum fault, Tibet. Earth and Planetary Science Letters 219, 255–269.

Le Breton, N., Thompson, A.B., 1988. Fluid-absent (dehydration) melting of biotite in metapelites in the early stages of crustal anatexis. Contributions to Mineralogy and Petrology 99, 226–237.

LeFort, P., Tongiorgi, M., Gaetani, M., 1994. Discovery of a crystalline basement and Early Ordovician marine transgression in the Karakorum mountain range, Pakistan. Geology 22, 941–944.

Leloup, P.H., Kienast, J.R., 1993. High-temperature in a major strike-slip shear zone: the Ailao Shan-Red River, People's Republic of China. Earth and Planetary Science Letters 118, 213–234.

Leloup, P.H., Lacassin, R., Tapponnier, P., Schärer, U., Zhong, Dalai, Liu, Xiaohan, Zhang, Liangshang, Ji, Shaocheng, Phan, Trong Trinh, 1995. The Ailao Shan-Red River Shear Zone (Yunnan, China), Tertiary transform boundary of Indochina. Tectonophysics 251, 3–84.

Leloup, P.H., Ricard, Y., Battaglia, J., Lacassin, R., 1999. Shear heating in continental strike-slip shear zones: model and field examples. Geophysical Journal of Interiors 136, 19–40.

Le Pichon, X., Henry, P., Goffé, B., 1997. Uplift of Tibet: from eclogites to granulites, implications for the Andean Plateau and the Variscan belt. Tectonophysics 273, 57–76.

Liu, Q., 1993. Paléoclimat et contraintes chronologiques sur les mouvements récents dans l'Ouest du Tibet: failles du Karakorum et de Longmu Co-Gozha Co, lac en pull-apart de Longmu Co et de Sumxi Co. Ph.D. Thesis, Paris University, 360 p.

Liu, Q., Avouac, J.P., Tapponnier, P., Zhang, Q., 1992. Holocene movement along the southern part of the Karakorum Fault. Abstracts, International symposium on the Karakorum and Kun Lun Mountains, Kashgar, China, 91.

Mahéo, G., Guillot, S., Blichert-Toft, J., Rolland, Y., Pêcher, A., 2002. A slab breakoff model for the Neogene thermal evolution of South Karakorum and South Tibet. Earth and Planetary Science Letters 195, 45–58.

Mahéo, G., Pêcher, A., Guillot, S., Rolland, Y., Delacourt, C., 2004. Ehumation of Neogene gneiss domes between oblique crustal boundaries in south Karakorum (northwest Himalaya, Pakistan). Geological Society of America Special Paper 380, 141–154.

Matte, P., Tapponnier, P., Arnaud, N., Bourjot, L., Avouac, J.P., Vidal, P., Liu, Qing, Pan, Yusheng, Wang, Yi, 1996. Tectonics of Western Tibet, between the Tarim and the Indus. Earth and Planetary Science Letters 142, 311–330.

Moody, J.B., Meye, D., Jenkins, J.E., 1983. Experimental characterization of the greenschist–amphibolite boundary in mafic systems. American Journal of Science 28, 48–92.

Murphy, M.A., Yin, A., Kapp, P., Harrison, T.M., Ding, Lin, Guo, Jinghui, 2000. Southward propagation of the Karakorum fault system, southwest Tibet: timing and magnitude of slip. Geology 28, 451–454.

Nabelek, P., Liu, M., Sirbescu, M., 2001. Thermal-rheological shear heating model for leucogranite generation, metamorphism, and deformation during the Proterozoic Trans-Hudson orogeny, Black Hills, South Dakota. Tectonophysics 342, 371–388.

Nitsch, K.H., 1971. Stabilitätsbeziehungen von Prehnit-und Pumpellyit-haltiger Paragenesen. Contributions to Mineralogy and Petrology 30, 240–260.

Parrish, R.P., Tirrul, R., 1989. U–Pb ages of the Baltoro granite, northwestern Himalaya, and implications for zircon inheritance and monazite U–Pb systematics. Geology 17, 1076–1079.

Peltzer, G., Tapponnier, P., 1988. Formation and evolution of strike-slip faults, rifts and basins during the India–Asia collision: an experimental approach. Journal of Geophysical Research 93, 15085–15117.

Petterson, M.G., Windley, B.F., 1991. Changing source regions of magmas and crustal growth in the Trans-Himalayas: evidence from the Chalt volcanics and Kohistan Batholith, Kohistan, northern Pakistan. Earth and Planetary Science Letters 102, 326–341.

Phillips, J.P., Parrish, R.R., Searle, M.P., 2004. Age constraints on ductile deformation and long-term slip rates along the Karakoram fault zone, Ladakh. Earth and Planetary Science Letters 226, 305–319.

Plyusnina, L.P., 1982. Geothermobarometry and geobarometry of plagioclase–hornblende bearing assemblages. Contributions to Mineralogy and Petrology 80, 140–146.

Pognante, U., 1990. Shoshonitic and ultrapotassic post-collisional dykes from northern Karakorum (Sinkiang, China). Lithos 26, 305–316.

Powell, R., Holland, T.J.B., 1988. An internally consistent thermodynamic dataset with uncertainties and correlations: 3. Applications to geobarometry, worked examples and computer program. Journal of Metamorphic Geology 6, 173–204.

Rex, A.J., Searle, M.P., Tirrul, R., Crawford, D.J., Prior, D.J., Rex, D.C., 1988. The geochemical and tectonic evolution of the central Karakoram, north Pakistan. Philosophical Transactions of the Royal Society London Series A 326, 229–255.

Rolland Y., 2002. From intra-oceanic convergence to post-collisional evolution: example of the India–Asia convergence in NW Himalaya, from Cretaceous to present. In: Rosenbaum, G., Lister, G.S. (Eds.), Reconstruction of the evolution of the Alpine-Himalayan orogeny. Journal of the Virtual Explorer 8. Available from: <http://www.virtualexplorer.com.au/VEjournal/2002Volumes/index.html>.

Rolland, Y., Pêcher, A., Picard, C., 2000. Mid-Cretaceous back-arc formation and Arc evolution along the Asian margin: the Shyok Suture Zone in northern Ladakh (NW Himalaya). Tectonophysics 325, 145–173.

Rolland, Y., Pêcher, A., 2001. The Pangong granulites of the Karakorum Fault (Western Tibet): vertical extrusion within a lithosphere-scale fault? Comptes Rendus Académie des Sciences Paris 332, 363–370.

Rolland, Y., Mahéo, G., Guillot, S., Pêcher, A., 2001. Tectono-metamorphic evolution of the Karakorum Metamorphic Complex (Dassu-Askole area, NE Pakistan): exhumation of mid-crustal HT–MP gneisses in a convergent context. Journal of Metamorphic Geology 19, 717–737.

Rolland, Y., Pêcher, A., Picard, C., Villa, I.M., Carrio, E., Oddone, M., 2002a. Precambrian and Ordovician series of the Karakorum Asian Margin (NW Himalaya): evidence for Early Paleozoic arc dynamics. Geodinamica Acta 15, 1–22.

Rolland, Y., Picard, C., Pêcher, A., Lapierre, H., Bosch, D., Keller, F., 2002b. The Ladakh Arc of NW Himalaya – slab melting and melt-mantle interaction during fast northward drift of Indian Plate. Chemical Geology 182, 139–178.

Rolland, Y., Carrio-Schaffhauser, E., Sheppard, S.M.F., Pêcher, A., Esclauze, L., 2006a. Metamorphic zoning and geodynamic evolution of an inverted crustal section (Karakorum margin, N Pakistan), evidence for two metamorphic events. International Journal of Earth Sciences 95, 288–305. doi:10.1007/s00531-005-0026-x.

Rolland, Y., Villa, I.M., Guillot, S., Mahéo, G., Pêcher, A., 2006b. Evidence for pre-Cretaceous history and partial Neogene (19–9 Ma) reequilibration in the Karakorum (NW Himalayan Syntaxis) from ^{40}Ar–^{39}Ar amphibole dating. Journal of Asian Earth Sciences 27, 371–391.

Schärer, U., Copeland, P., Harrison, T.M., Searle, M.P., 1990a. Age, cooling history and origin of post-collisional leucogranites in the Karakorum batholith: a multi-system isotope study, N. Pakistan. Journal of Geology 98, 233–251.

Schärer, U., Tapponnier, P., Lacassin, R., Leloup, P.H., Zhong, Dalai, Ji, Shaocheng, 1990b. Intraplate tectonics in Asia: a precise age for large-scale Miocene movement along the Ailao Shan-Red River shear zone, China. Earth and Planetary Science Letters 97, 65–77.

Schärer, U., Zang, Lian-Sheng, Tapponnier, P., 1994. Duration of strike-slip movements in large shear zones: the Red River belt, China. Earth and Planetary Science Letters 126, 379–397.

Schiffman, P., Liou, J.G., 1980. Synthesis and stability relations of Mg–Al pumpellyite, $Ca_4Al_5MgSi_6O_{21}(OH)_7$. Journal of Petrology 21, 441–474.

Searle, M.P., 1996. Geological evidence against large scale pre-Holocene offsets along the Karakorum Fault: implications for the limited extrusion of the Tibetan Plateau. Tectonics 15, 171–186.

Searle, M.P., Phillips, R.J., 2004. A comment on "large-scale geometry, offset, and kinematic evolution of the Karakoram fault, Tibet" by R. Lacassin et al.. Earth and Planetary Science Letters 229, 155–158.

Searle, M.P., Weinberg, R.F., Dunlap, W.J., 1998. Transpressional tectonics along the Karakorum fault zone, Northern Ladakh: constraints on Tibetan extrusion. Geological Society London Special Publication 135, 307–326.

Searle, M.P., Asif Khan, M., Fraser, J.E., Gough, S.J., 1999. The tectonic evolution of the Kohistan–Karakorum collision belt along the Karakorum Highway transect, north Pakistan. Tectonics 18, 929–949.

Spear, F.S., 1981. An experimental study of hornblende stability and compositional variability in amphibolite. American Journal of Science 281, 697–734.

Spear, F.S., 1993. Metamorphic Phase Equilibria and Pressure–Temperature–Time Paths. Mineralogical Society of America, Monograph Series.

Spear, F.S., Cheney, J.T., 1989. A petrogenetic grid for pelitic schists in the system SiO_2–Al_2O_3–FeO–MgO–K_2O–H_2O. Contributions to Mineralogy and Petrology 101, 149–164.

Tapponnier, P., Molnar, P., 1977. Active faulting and tectonics in China. Journal of Geophysical Research 82, 2905–2930.

Tapponnier, P., Peltzer, G., Armijo, R., 1986. On the mechanics of the collision between India and Asia. Geological Society Special Publication London 19, 115–157.

Tapponnier, P., Lacassin, R., Leloup, P.H., Schärer, U., Dalai, Z., Wu, Haiwei, Liu, Xiaohan, ji, Shaocheng, Zhang, Lianshang, Zhong, Jiayou, 1990. The Ailoa Shan/

Red River metamorphic belt: tertiary left-lateral shear between Indochina and South China. Nature 343, 431–437.

Thompson, A.B., 1982. Dehydration melting of pelitic rocks and the generation of H_2O-saturated granitic liquids. American Journal of Science 282, 1567–1595.

Treloar, P.J., Petterson, M.G., Jan, M.Q., Sullivan, M.A., 1996. A re-evaluation of the stratigraphy and evolution of the Kohistan Arc sequence, Pakistan Himalaya: implications for magmatic and tectonic arc-building processes. Journal of the Geological Society London 153, 681–693.

Valli, F., Arnaud, N., Paquette, J.L., Leloup, P.H., Lacassin, R., Li, H., Guillot, S., Tapponnier, P., Xu, Z., Deloule, E., 2003. New age constraints on the evolution of the Karakorum fault, west Tibet. EGS–AGU–EUG Joint Assembly. abstract 8377.

Vielzeuf, D., 1984. Relations de phases dans le faciès granulite et implications géodynamiques. Unpublished Thesis, Clermont–Ferrand II University.

Vielzeuf, D., Holloway, J.R., 1988. Experimental determination of the fluid-absent melting reactions in the pelitic system. Consequences for crustal differentiation. Contributions to Mineralogy and Petrology 98, 257–276.

Villa, I.M., Ruffini, R., Rolfo, F., Lombardo, B., 1996. Diachronous metamorphism of the Ladakh Terrane at the Karakorum–Nanga Parbat–Haramosh junction (NW Baltistan, Pakistan). Schweizeriche Mineraleralogische Petrographische Mittelungen 76, 245–264.

Villa, I.M., Hermann, J., Müntener, O., Trommsdorff, V., 2000. ^{39}Ar–^{40}Ar dating of multiply zoned amphibole generations (Malenco, Italian Alps). Contributions to Mineralogy and Petrology 140, 363–381.

Weinberg, R.F., Searle, M.P., 1998. The Pangong Injection Complex, Indian Karakoram: a case of pervasive granite flow through hot viscous crust. Journal of the Geological Society London 155, 883–891.

Weinberg, R.F., Dunlap, W., Whitehouse, M., 2000. New field, structural and geochronological data from the Shyok and Nubra valleys, northern Ladakh: linking Kohistan to Tibet. In: Khan, M.A., Treloar, P.J., Searle, M.P., Jan, M.Q. (Eds.), Tectonics of the Nanga Parbat Syntaxis and the Western Himalaya, vol. 170. Geological Society London Special Publication, pp. 253–275.

Wittlinger, G., Tapponnier, P., Poupinet, G., Mei, J., Danian, S., Herquel, G., Masson, F., 1998. Tomographic evidence for localized lithospheric shear along the Altyn Tagh Fault. Science 282, 74–76.

Xu, R., Schärer, U., Allègre, C.J., 1985. Magmatism and metamorphism in the Lhasa Block (Tibet): a geochronological study. Journal of Geology 93, 41–57.

Yin, J.X., Xu, J.T., Liu, C.G., Li, H., 1988. The Tibetan Plateau: regional stratigraphic context and previous work. In: Chang, C.F. et al. (Eds.), The Geological Evolution of Tibet, vol. 327. Royal Society of London Philosophical Transactions, pp. 5–52.

Zanchi, A., Poli, S., Fumagalli, P., Gaetani, M., 2000. Mantle exhumation along the Tirich Mir Fault (NW Pakistan): pre-mid-Cretaceous accretion of the Karakorum Terrane to the Eurasian margin. In: Khan, M.A., Treloar, P.J., Searle, M.P., Jan, M.Q. (Eds.), Tectonics of the Nanga Parbat Syntaxis and the Western Himalaya, vol. 170. Geological Society London Special Publications, 237-252.

Zeitler, P.K., Chamberlain, C.P., Smith, H.A., 1993. Synchronous anatexis, metamorphism and rapid exhumation at Nanga Parbat (Pakistan Himalaya). Geology 21, 347–350.

Please cite this article in press as: Rolland, Y. et al., Syn-kinematic emplacement of the Pangong metamorphic and magmatic complex along the Karakorum Fault (N Ladakh) ..., Journal of Asian Earth Sciences (2008), doi:10.1016/j.jseaes.2008.03.009